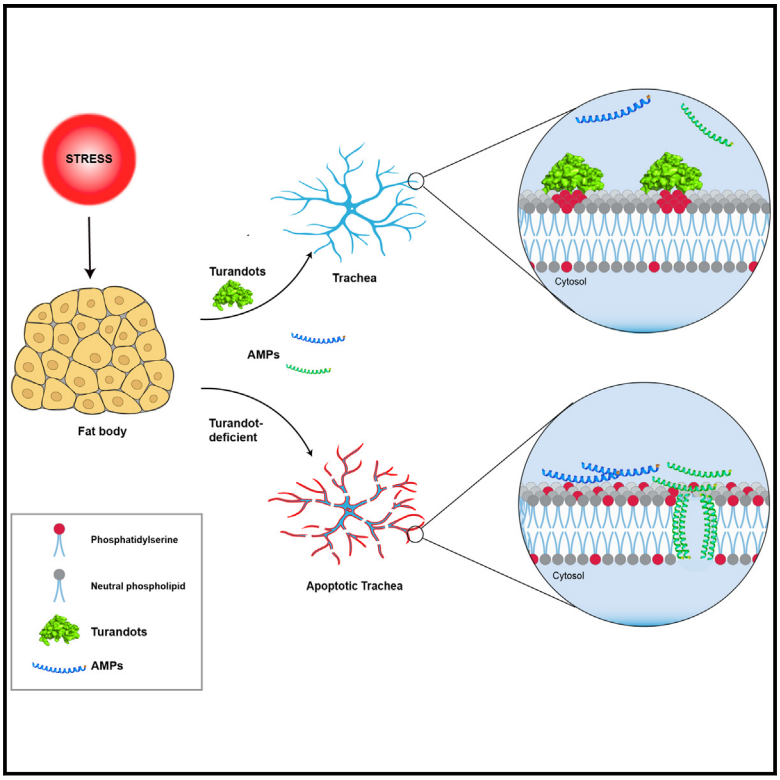
Article

Current Biology

A humoral stress response protects *Drosophila* tissues from antimicrobial peptides

Graphical abstract



Authors

Samuel Rommelaere, Alexia Carboni, Juan F. Bada Juarez, ..., Matteo Dal Peraro, Chan Cao, Bruno Lemaitre

Correspondence

samuel.rommelaere@epfl.ch (S.R.), bruno.lemaitre@epfl.ch (B.L.)

In brief

Combating infection without causing host damage is a delicate challenge. Rommelaere et al. show that a family of cytoprotective proteins, the Turandots, alleviates antimicrobial peptide toxicity against *Drosophila* tissues that expose phosphatidylserine. Turandots mask phosphatidylserine, preventing membrane pore formation by antimicrobial peptides.

Highlights

- Trachea expose phosphatidylserine, making them sensitive to AMPs
- Turandots are secreted proteins that protect the respiratory epithelium
- Turandots shield phosphatidylserine, preventing pore formation by AMPs
- Turandots favor *Drosophila* resilience to stress by preventing immunopathology

Rommelaere et al., 2024, Current Biology *34*, 1426–1437
April 8, 2024 © 2024 The Authors. Published by Elsevier Inc.
https://doi.org/10.1016/j.cub.2024.02.049

CellPress

CellPress
OPEN ACCESS

Current Biology

Article

A humoral stress response protects *Drosophila* tissues from antimicrobial peptides

Samuel Rommelaere,[1,*] Alexia Carboni,[1] Juan F. Bada Juarez,[2] Jean-Philippe Boquete,[1] Luciano A. Abriata,[2] Fernando Teixeira Pinto Meireles,[2] Verena Rukes,[2] Crystal Vincent,[3] Shu Kondo,[4] Marc S. Dionne,[5] Matteo Dal Peraro,[2] Chan Cao,[6] and Bruno Lemaitre[1,7,8,*]

[1]Global Health Institute, School of Life Science, École Polytechnique Fédérale de Lausanne (EPFL), 1015 Lausanne, Switzerland
[2]Institute of Bioengineering, School of Life Science, École Polytechnique Fédérale de Lausanne (EPFL), 1015 Lausanne, Switzerland
[3]Department of Biochemistry, School of Biological and Behavioural Sciences, Queen Mary University of London, E1 4NS London, UK
[4]Department of Biological Science and Technology, Faculty of Advanced Engineering, Tokyo University of Science, 162-8601 Tokyo, Japan
[5]Centre for Bacterial Resistance Biology and Department of Life Sciences, Imperial College London, London SW7 2AZ, UK
[6]Department of Inorganic and Analytical Chemistry, Chemistry and Biochemistry, University of Geneva, 1211 Geneva, Switzerland
[7]X (formerly Twitter): @BrunoLemaitre3
[8]Lead contact
*Correspondence: samuel.rommelaere@epfl.ch (S.R.), bruno.lemaitre@epfl.ch (B.L.)
https://doi.org/10.1016/j.cub.2024.02.049

SUMMARY

7An efficient immune system must provide protection against a broad range of pathogens without causing excessive collateral tissue damage. While immune effectors have been well characterized, we know less about the resilience mechanisms protecting the host from its own immune response. Antimicrobial peptides (AMPs) are small, cationic peptides that contribute to innate defenses by targeting negatively charged membranes of microbes. While protective against pathogens, AMPs can be cytotoxic to host cells. Here, we reveal that a family of stress-induced proteins, the Turandots, protect the *Drosophila* respiratory system from AMPs, increasing resilience to stress. Flies lacking *Turandot* genes are susceptible to environmental stresses due to AMP-induced tracheal apoptosis. Turandot proteins bind to host cell membranes and mask negatively charged phospholipids, protecting them from cationic pore-forming AMPs. Collectively, these data demonstrate that Turandot stress proteins mitigate AMP cytotoxicity to host tissues and therefore improve their efficacy.

INTRODUCTION

Multiple mechanisms have evolved in animals to ensure homeostasis upon biotic and abiotic stresses. These include the production of heat shock proteins, cryoprotectants, antioxidants, the unfolded protein response, and compensatory proliferation to replace dead cells, all of which contribute to resilience in stressful conditions.[1–3] These stress pathways also play an active role in defense against microbes, not only to prevent pathogen-induced damage but also to protect the host from deleterious effects of the immune response itself.

Antimicrobial peptides (AMPs) are small, cationic, usually amphipathic peptides that contribute to innate immune defense in plants and animals.[4–6] Most display potent antimicrobial activity *in vitro* by disrupting negatively charged microbial membranes. Host membranes of animals typically have a neutral charge and are therefore not affected by pore-forming AMP activity. However, AMPs can be cytotoxic to host cells in certain contexts when expressed at high levels.[7–9] Hypotheses suggest that AMPs could target cell membranes that become negatively charged due to translocation of the phospholipid phosphatidylserine (PS) to the outer leaflet upon stress.[10,11] To date, little is known of host mechanisms that protect tissues against AMP collateral damage during the immune response.

AMPs are well characterized in the fruit fly *Drosophila melanogaster* where they enable resistance of microbial infections and shape the microbiota.[4,12,13] In this insect, systemic infection triggers massive secretion of multiple AMPs by the fat body, an equivalent of the mammalian liver. AMPs can also be induced by abiotic stressors such as osmotic stress or desiccation.[14,15] In *Drosophila*, the *Turandot* (*Tot*) gene family produces eight small secreted proteins that are highly expressed in AMP-like patterns during stress and immune responses.[16,17] Although expression of *Tot* genes is widely used as a readout of the stress response,[18–20] their molecular function is unknown. Here, we show that Turandot proteins are humoral factors that protect host tissues, notably the respiratory epithelium, from AMPs, contributing to stress resilience, and host defense.

RESULTS

Turandot-deficient flies have low resilience to stress

Because of their sequence similarity and overlapping expression patterns, we anticipated functional redundancies among the eight *Turandot* genes. To assess their function, we generated compound mutants inactivating up to 6 out of 8 Turandot genes, excluding TotE and TotF. These two genes are expressed in embryos, suggesting a role in early development (Flybase). We first

 © 2024 The Authors. Published by Elsevier Inc.
This is an open access article under the CC BY license (http://creativecommons.org/licenses/by/4.0/).

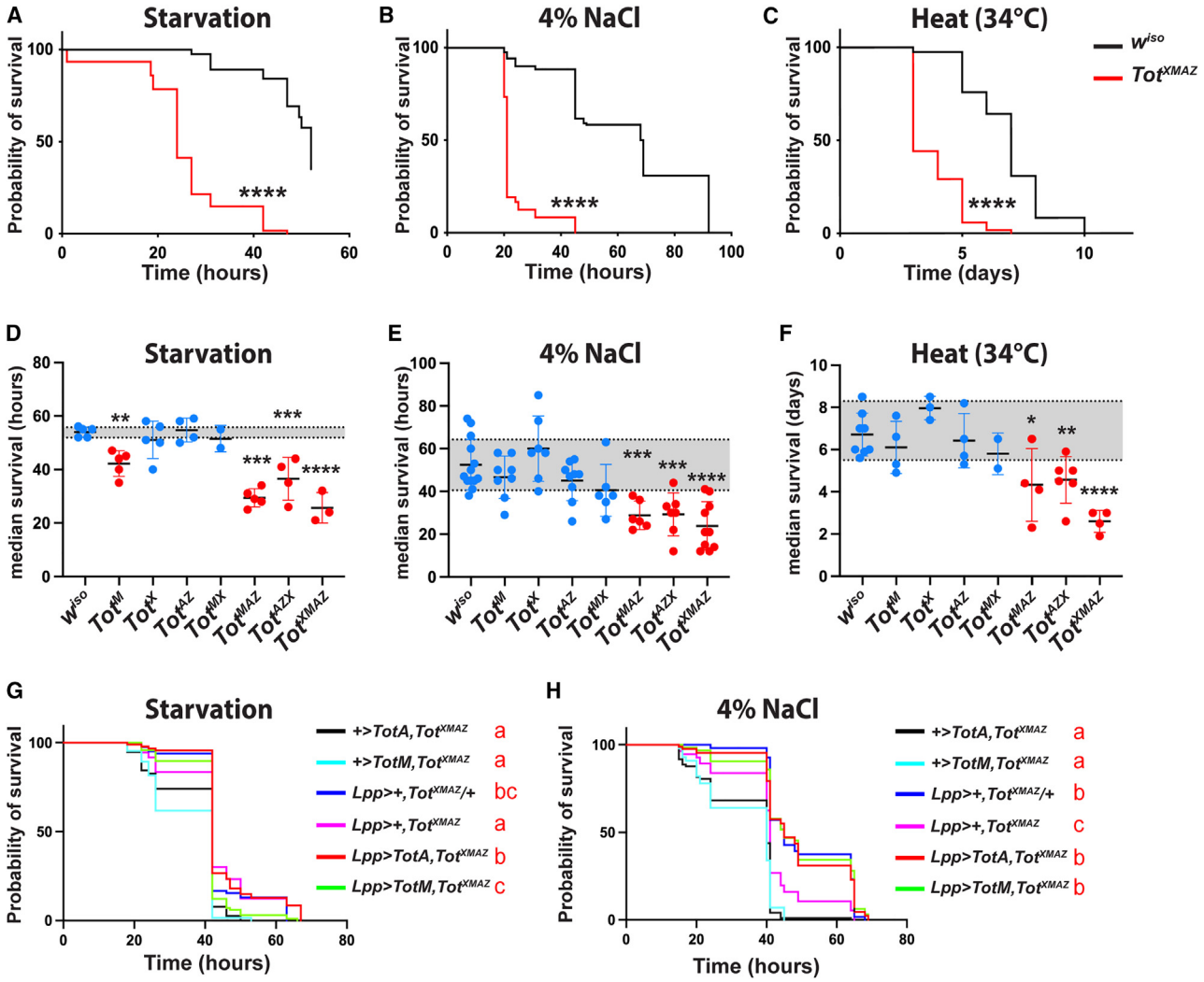


Figure 1. Turandot-deficient flies are susceptible to stress

(A–C) Survival of wild-type w^{iso} control (black, n = 120) and Tot^{XMAZ} flies (red, n = 120) maintained on agar only (A) or on food containing 4% NaCl (B) or at 34°C (C).

(D–F) Median survival of different *Tot*-deficient fly lines to starvation (D), osmotic stress (E), or heat stress (F). Each dot represents a single experiment. Black lines indicate the median, and error bars represent the standard deviation (SD). Gray intervals highlight the variance of the w^{iso} line. Genotypes in red are significantly different from w^{iso} line (ordinary one-way ANOVA followed by a Dunnett's multiple comparisons test; ns, not significant; $p \geq 0.05$, * for p between 0.01 and 0.05; ** for p between 0.001 and 0.01, *** for p between 0.0001 and 0.001, ****$p \leq 0.0001$).

(G and H) Survival upon starvation (G) or osmotic stress (H) of +>*TotA;Tot*^{XMAZ} (black), +>*TotM;Tot*^{XMAZ} (light blue), *lpp*>+;*Tot*^{XMAZ}/+ (blue), *lpp*>+;*Tot*^{XMAZ} (pink), *lpp*>*TotA;Tot*^{XMAZ} (red), and *lpp*>*TotM;Tot*^{XMAZ} (green). Results shown are a pool of 3 independent experiments. (****$p < 0.0001$; Cox proportional hazard [CoxPH] test, followed by Benjamini-Hochberg correction when applicable; in this case, a compact letter display was used to show the statistics; see STAR Methods). See also Figure S1.

generated a mutant deleted for a genomic cluster of four genes (*TotA*, *TotB*, *TotC*, and *TotZ*) called Tot^{AZ}. In this mutant, we then inactivated *TotM*, *TotX*, or both, creating the Tot^{MAZ}, Tot^{AZX}, or Tot^{XMAZ} lines, respectively. *Tot*-deficient flies were viable and fertile. The expression pattern of *Turandot* genes implied that they might play an important role against a broad range of stresses.[16,18,19,21,22] We therefore subjected *Tot*-deficient flies to biotic and abiotic challenges. Tot^{XMAZ} animals showed a mild, yet not significant, susceptibility to systemic infection with *Drosophila* C virus, *Pectobacterium carotovorum carotovorum* (*Ecc15*) or *Enterococcus faecalis* (Figures S1A–S1F), as compared with isogenic wild-type flies. Strikingly, Tot^{XMAZ} flies were more susceptible to starvation, osmotic, and heat stresses than wild-type animals, (Figures 1A–1C). Tot^{AZ} mutants showed a mild and variable susceptibility to these stresses, while both Tot^{MAZ} and Tot^{AZX} displayed a strong and consistent susceptibility to these challenges. Tot^{AZX} and Tot^{XMAZ} flies were similarly susceptible to all challenges tested (Figures 1D–1F). Thus, we mostly used Tot^{AZX} and Tot^{XMAZ} flies to address Turandot function in the following genetic characterization (see STAR Methods). Overexpression of *TotA* or *TotM* alone in the fat body of Tot^{XMAZ} flies almost fully rescued resistance to starvation and osmotic stress (Figures 1G and 1H), confirming that the susceptibility is caused by *Tot* deficiency. Interestingly, ubiquitous overexpression of

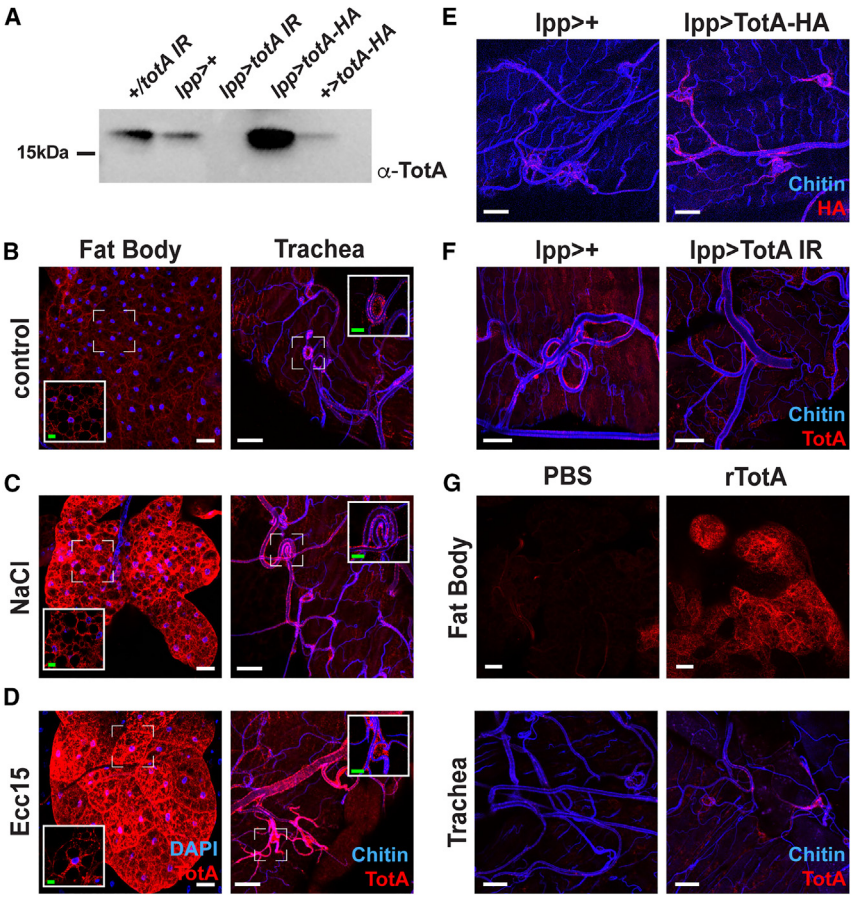


Figure 2. Fat-body-secreted Turandots bind to trachea

(A) Anti-TotA western blot analysis of hemolymph from animals overexpressing TotA-HA or TotA RNAi in the fat body.

(B–D) Anti-TotA immunostaining of fat bodies (left) or gut trachea (right) of unchallenged flies (B) or flies exposed to osmotic stress (NaCl, C) or *Ecc15* infection (D). Insets show high magnification of the area defined by the white dotted square. Image brightness in these insets was adjusted to highlight the punctate structures.

(E) Anti-HA immunostaining of trachea from control (left) or TotA-HA-overexpressing (right) flies.

(F) Anti-TotA immunostainings of trachea from wild-type flies (left) or flies overexpressing TotA RNAi in the fat body (right).

(G) Anti-TotA immunostaining of fat bodies (upper) and trachea (lower) from flies injected with PBS (left) or with recombinant TotA (right). Blue, chitin; red, TotA or TotA-HA. Scale bars: white, 20 μm; green, 5 μm.

See also Figure S2.

TotA in the *Tot*^{XMAZ} background failed to rescue the survival phenotype, suggesting that ectopic or excessive expression of *TotA* is detrimental to flies (Figures S1G and S1H). Together, these data demonstrate that *Turandot* genes are required for optimal resilience to a broad set of environmental challenges.

Secreted TotA binds to trachea

We next analyzed the expression pattern of Tot proteins, focusing on TotA. Western blot with an anti-TotA polyclonal antibody confirmed the secretion of this protein into the hemolymph (insect circulatory fluid) (Figure 2A). Immunostaining also revealed the presence of TotA in the fat body and, to a lesser extent, on trachea (insect respiratory system) and visceral muscles of unchallenged flies (Figures 2B, S2A, and S2B). TotA was mostly localized at the plasma membrane and in intracellular punctae (Figure 2B). Osmotic stress and bacterial infection increased TotA staining in the fat body and the trachea (Figures 2C and 2D). Because TotA is weakly expressed in trachea in basal conditions (Figure S2C), we hypothesized that this staining could result from tracheal binding of TotA secreted by the fat body. Consistent with this, hemagglutinin (HA)-tagged TotA was observed on trachea when remotely expressed in the fat body (Figure 2E). Similar results were obtained upon overexpression of HA-tagged versions of TotB, TotE, TotF, and TotM, suggesting that all fat-body-derived Tots bind to trachea (Figures S2D and S2E). Conversely, knocking down TotA in the fat body reduced TotA staining of the trachea (Figure 2F). Finally, we injected recombinant TotA protein into *TotA*-deficient animals and detected it on the plasma membranes of the fat body and trachea (Figure 2G). These data show that upon stress, TotA is secreted into the hemolymph and binds to fat and tracheal cells.

Turandots maintain tissue oxygenation by protecting trachea from apoptosis

The binding of fat-body-produced Tot proteins to trachea was unexpected. Therefore, we further investigated the role of Turandots in the respiratory epithelium upon stress, focusing on the tracheal network around the gut. We found that *Tot*^{XMAZ} mutant flies had fewer terminal tracheal cells (TTCs), and reduced tracheal coverage of the midgut compared with wild-type flies, as revealed by chitin autofluorescence[23] (Figures 3A–3C) or a *dSRF>GFP* tracheal reporter[24] (Figure 3D). Overexpressing *TotA* in the fat body of *Tot*^{XMAZ} flies was sufficient to restore TTC numbers comparable to wild-type flies (Figure 3E). As we did not detect any anatomical defect in the trachea of *Tot*^{XMAZ} larvae (Figure S3), we speculated that Turandots were required during metamorphosis to ensure proper tracheal morphogenesis, consistent with the high expression of *Tot* at the pupal stage.[25] Adult tracheal branching is modulated by nutrient cues and infection,[23,26,27] which prompted us to test whether stress could affect tracheation. Osmotic stress significantly reduced TTC number and tracheal coverage in both wild-type and *Tot*^{XMAZ} animals, showing that the tracheal system is intrinsically vulnerable to environmental stresses (Figures 3B and 3C).

The main function of trachea is tissue oxygenation and CO_2 disposal.[28] As expected, the reduced tracheation observed in *Tot*-mutant flies resulted in lower tissue oxygenation, as measured by a transgene expressing a fluorescent oxygen sensor[29] (Figure 3F). Furthermore, flow-through respirometry revealed that *Tot*^{XMAZ} flies consumed less O_2 and produced less CO_2 than the wild type (Figure 3G). These results

CellPress
OPEN ACCESS

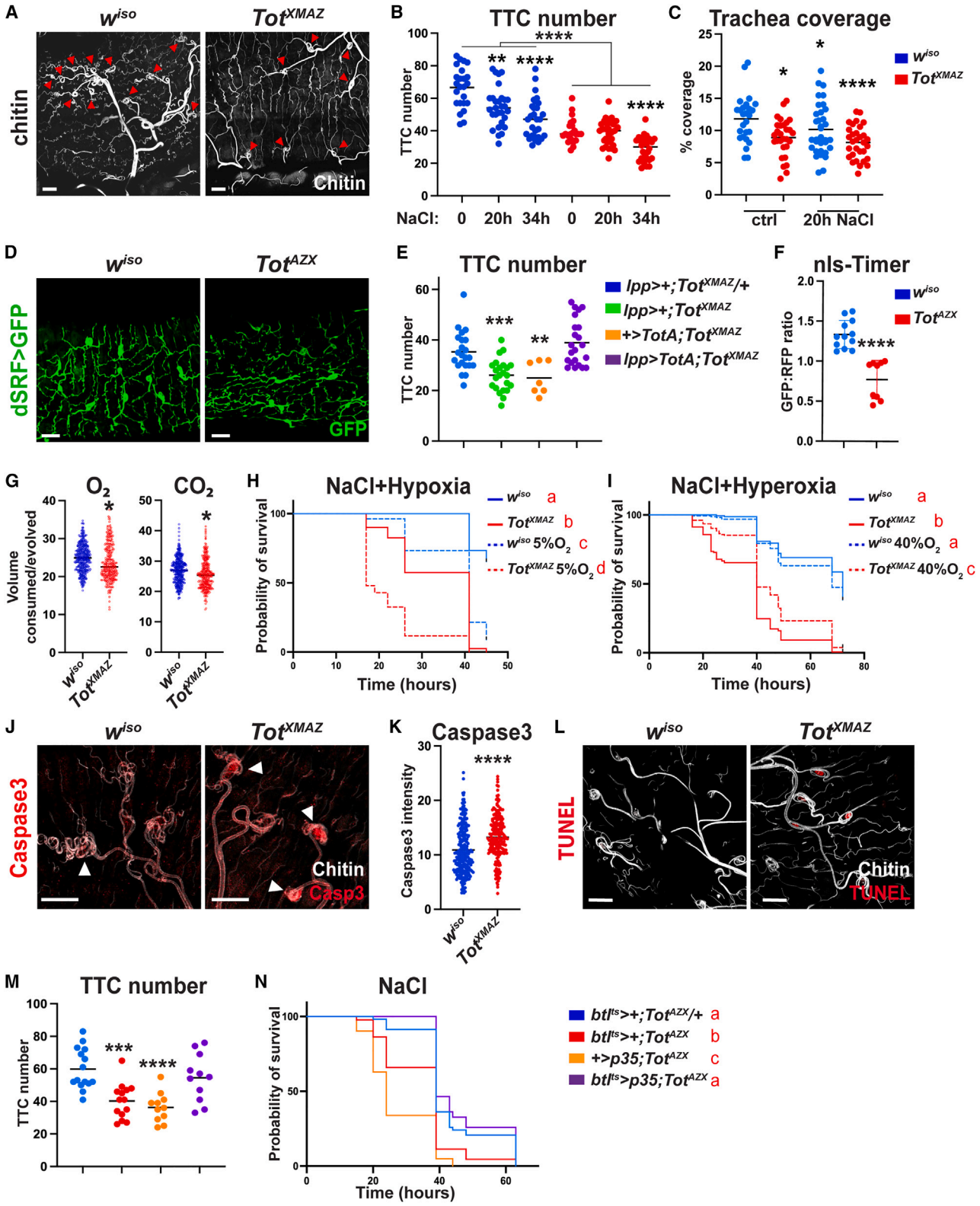


Figure 3. Turandots promote resilience to stress by preventing tracheal apoptosis

(A) Chitin autofluorescence (gray) of gut trachea in w^{iso} (left) or Tot^{XMAZ} (right) flies. Red arrowheads indicate TTC.

(B and C) Quantification of gut TTC (B) and tracheal coverage (C) from w^{iso} (blue) and Tot^{XMAZ} (red) flies in unchallenged conditions or exposed to osmotic stress for 20 or 34 h.

(legend continued on next page)

suggested that O_2 delivery may limit the ability of *Tot*-deficient flies to cope with stress. To test this hypothesis, we exposed flies to osmotic stress or bacterial infection at varying oxygen pressures. Hypoxia increased the susceptibility of both wild-type and Tot^{XMAZ} flies to osmotic stress and bacterial infection (Figures 3H and S1D–S1F), highlighting the importance of oxygenation to resist these stresses. Strikingly, hyperoxia partially rescued Tot^{XMAZ} susceptibility to osmotic stress (Figure 3I). These data demonstrate that Turandot-mediated support of oxygen delivery by trachea is critical to survive environmental stress.

Because *Tot*-deficient flies had reduced TTCs, we hypothesized that these cells may undergo apoptosis. Consistent with this, we observed increased cleaved caspase-3 and terminal deoxynucleotidyl transferase dUTP nick-end labeling (TUNEL) in trachea of *Tot*-deficient animals upon osmotic stress, as compared with wild-type flies (Figures 3J–3L). Conversely, expression of the apoptosis inhibitor p35[30] in trachea restored wild-type TTC numbers in Tot^{AZX} animals (Figure 3M) and restored resilience to osmotic stress (Figure 3N). These results show that Turandot proteins maintain oxygen supply upon stress by preventing tracheal cell apoptosis.

Turandots prevent PS-dependent tracheal cell killing

Since TTC appeared to die from apoptosis in *Tot*-deficient flies, we looked at the presence of PS, an early marker of cell death.[10,11] PS is usually confined to the cytoplasmic leaflet of the membrane but becomes exposed upon apoptosis. PS asymmetry is maintained by flippases of the P4-ATPase family, while scramblases promote PS exposure on the outer layer of the membrane.[31,32] A transgene expressing annexin-V-GFP revealed increased levels of PS at the surface of tracheal membranes of *Tot*-deficient flies upon osmotic stress, as compared with wild-type flies (Figures 4A and 4B). Unexpectedly, we found that both wild-type and *Tot*-mutant trachea spontaneously exposed measurable amounts of PS compared with other tissues, even without external challenge (Figure 4C). Strong annexin V staining was restricted to trachea and some muscles (Figures S4A–S4C). We then explored whether the high PS exposure on tracheal cells could explain their susceptibility to stress. Overexpressing the mouse scramblase *xkr8* in trachea of wild-type flies to increase PS exposure reduced TTC numbers and resilience to osmotic stress (Figures 4D and 4E). Conversely, lowering levels of PS exposed on trachea by knocking down *scramblase 1* in *Tot*-deficient flies restored normal TTC numbers and reduced susceptibility to stress (Figures 4F and 4G). Collectively, these results indicate that high constitutive PS exposure on trachea contributes to their vulnerability to stressful conditions.

TotA prevents PS-dependent apoptosis of trachea by AMPs

As PS is negatively charged, exposure on the outer leaflet is expected to sensitize cells to damage by cationic pore-forming AMPs.[4,8,33] We hypothesized that Tots may promote tracheal survival by preventing AMP-dependent cell death. To test this model, we monitored tracheal morphology in immune-challenged flies expressing high levels of AMPs. Infection with heat-killed bacteria decreased TTC number in wild-type animals, showing that the innate immune response adversely impacts trachea survival. Strikingly, neither Imd-pathway-deficient flies ($Relish^{E20}$),[34] which fail to express most AMPs, nor flies lacking 14 AMP genes ($\Delta AMP14$)[35] showed a reduction in TTC number after infection with heat-killed bacteria (Figure 5A). Similarly, fat-body-specific Imd pathway activation by overexpression of the peptidoglycan receptor protein LC (PGRP-LC) receptor reduced TTC number and resilience to osmotic stress (Figures 5B and 5C). These observations strongly suggested that AMPs directly kill tracheal cells during the immune response. We thus overexpressed individual AMPs in the fat body and tested their impact on TTC number. Immunostaining revealed binding of Defensin, Diptericin A, and Drosomycin to trachea (Figure S4D). Strikingly, overexpression of any of these AMPs was sufficient to reduce TTC number (Figure 5D). Similarly, injection of purified Cecropin A (CecA) drastically decreased TTC number in both wild-type and Tot^{XMAZ} animals, further reinforcing the notion that AMPs directly kill tracheal cells (Figure 5E). We next tested whether tracheal killing by AMPs relied on PS exposure. The reduction of TTC numbers and the vulnerability to stress of flies displaying high PS exposure due to the overexpression of *xkr8* in trachea was rescued in absence of Cecropins, a major class of AMPs[35,36] (Figures 5F and 5G). These data reveal that AMPs kill tracheal cells in a PS-dependent manner, leading to reduced resilience to osmotic stress. Assuming that Tots protect against AMP cytotoxic activity, we expected that removing AMP genes would be sufficient to reduce the vulnerability of *Tot*-deficient flies to stress. To test this notion, we generated a fly line simultaneously lacking six Tots and 12 AMPs and monitored tracheation and stress resilience in these

(D) Anti-GFP immunostaining (green) of gut trachea from *dsrf>GFP* (left) or *dsrf>GFP,*Tot^{AZX} (right) flies.
(E) Expression of TotA by the fat body Gal4 driver (*lpp-Gal4*) restores wild-type TTC counts in Tot^{XMAZ} flies.
(F) Ratiometric analysis of the oxygen *nls-timer* fluorescence in wild-type (blue) or Tot^{AZX} flies (red).
(G) O_2 consumption (left) and CO_2 production (right) of w^{iso} (blue) or Tot^{XMAZ} (red) flies.
(H and I) Survival to osmotic stress of w^{iso} (blue) and Tot^{XMAZ} (red) flies kept in normoxia (solid line), hypoxia (dashed line, H) or hyperoxia (dashed line, I).
(J) Cleaved caspase-3 (red, arrowheads) staining of trachea (chitin, white) from w^{iso} (left) or Tot^{XMAZ} (right) flies exposed to osmotic stress.
(K) Quantification of caspase-3 staining intensity in TTC from w^{iso} (blue) or Tot^{XMAZ} (red) flies fed NaCl food.
(L) TUNEL staining (red) staining of trachea (chitin, white) from w^{iso} (left) or Tot^{XMAZ} (right) flies exposed to osmotic stress.
(M and N) Gut TTC quantification (M) and survival to osmotic stress (N) of Tot^{AZX} flies overexpressing p35 in trachea using the *btl-Gal4* driver. Scale bars: 20 μm. Histograms: horizontal bar indicates the median, error bars represent the SD and each dot represents an independent animal, except in (K). Survival plots show a pool of at least 3 independent experiments. Statistics: ordinary one-way ANOVA followed by a Dunnett's multiple comparisons test (B, C, and E); Mann-Whitney test (F and K); Welch two sample t test (G); CoxPH test followed by Benjamini-Hochberg corrections (H and I). ns, not significant; $p \geq 0.05$, * for p between 0.01 and 0.05; ** for p between 0.001 and 0.01, *** for p between 0.0001 and 0.001, ****$p \leq 0.0001$.
See also Figure S3.

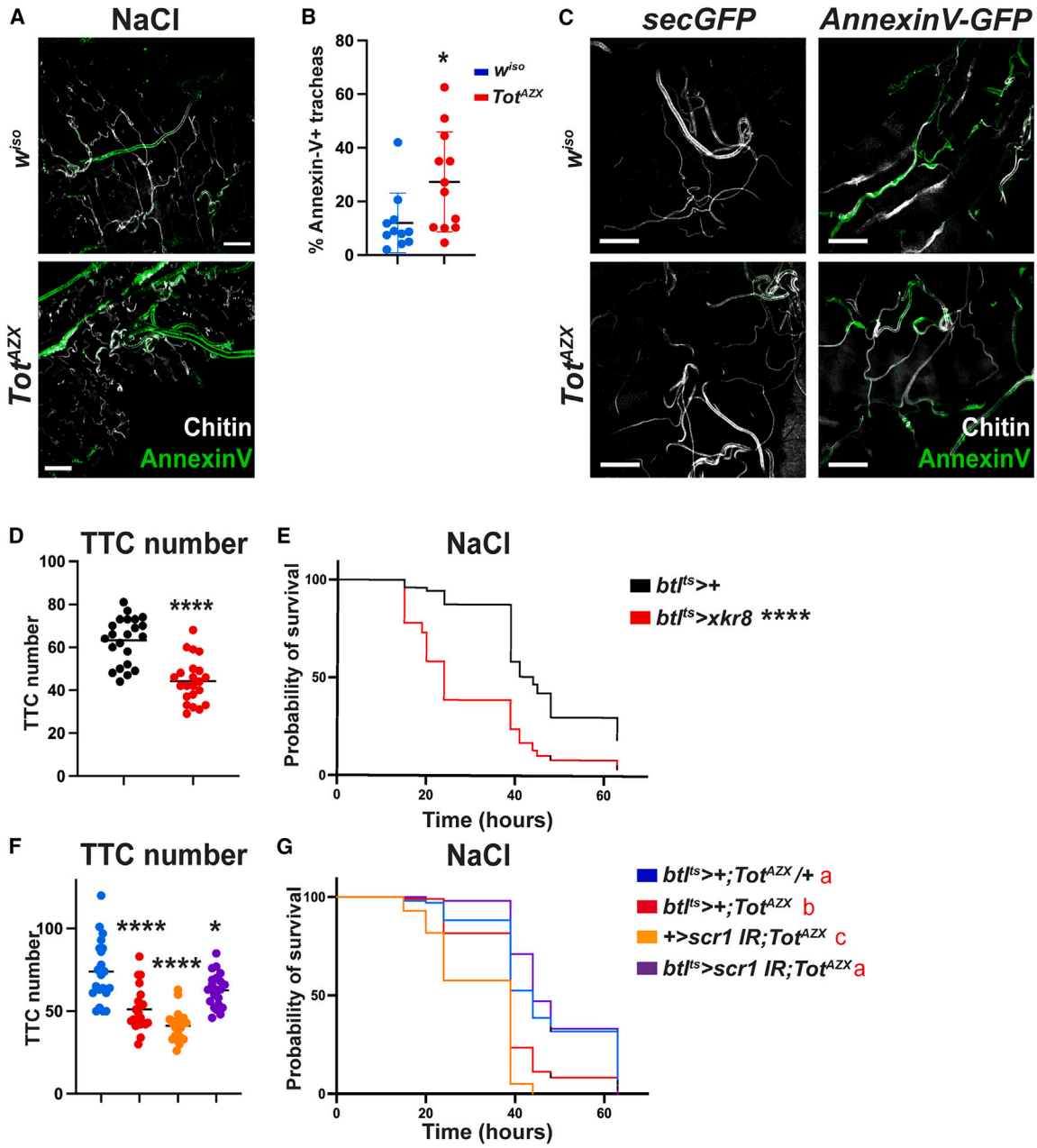


Figure 4. Turandots prevent PS-dependent tracheal cell killing

(A) Anti-GFP (green) immunostaining of trachea from control (upper, *lpp>AnnexinV-GFP*) or Tot-deficient (lower, *lpp>AnnexinV-GFP;Tot*^{AZX}) flies exposed to osmotic stress.

(B) Quantification of the tracheal surface stained by annexin V in control (blue) and Tot-deficient (red) flies fed NaCl food.

(C) Immunostaining of trachea from control (upper) and *Tot*-deficient flies (lower) overexpressing a secreted GFP (secGFP) (left) or annexin V-GFP (right) in the fat body. White, chitin; green, GFP; Scale bars: 20 μm.

(D and E) Quantification of TTC numbers (D) and survival to osmotic stress (E) of wild-type flies overexpressing *xkr8* in trachea with the *btl*^{ts} driver.

(F and G) Quantification of TTC numbers (F) and survival to osmotic stress (G) of *Tot*^{AZX} flies overexpressing *scramblase 1* RNAi in trachea with the *btl*^{ts} driver.

Histograms: horizontal bar indicates the median, error bars represent the SD, and each dot represents an independent animal. Survival plots show a pool of at least 3 independent experiments. Statistics: Mann-Whitney test (B and D); ordinary one-way ANOVA followed by a Dunnett's multiple comparisons test (F); CoxPH test followed by Benjamini-Hochberg correction (E and G). *$p \geq 0.05$; ****$p \leq 0.0001$.

See also Figure S4.

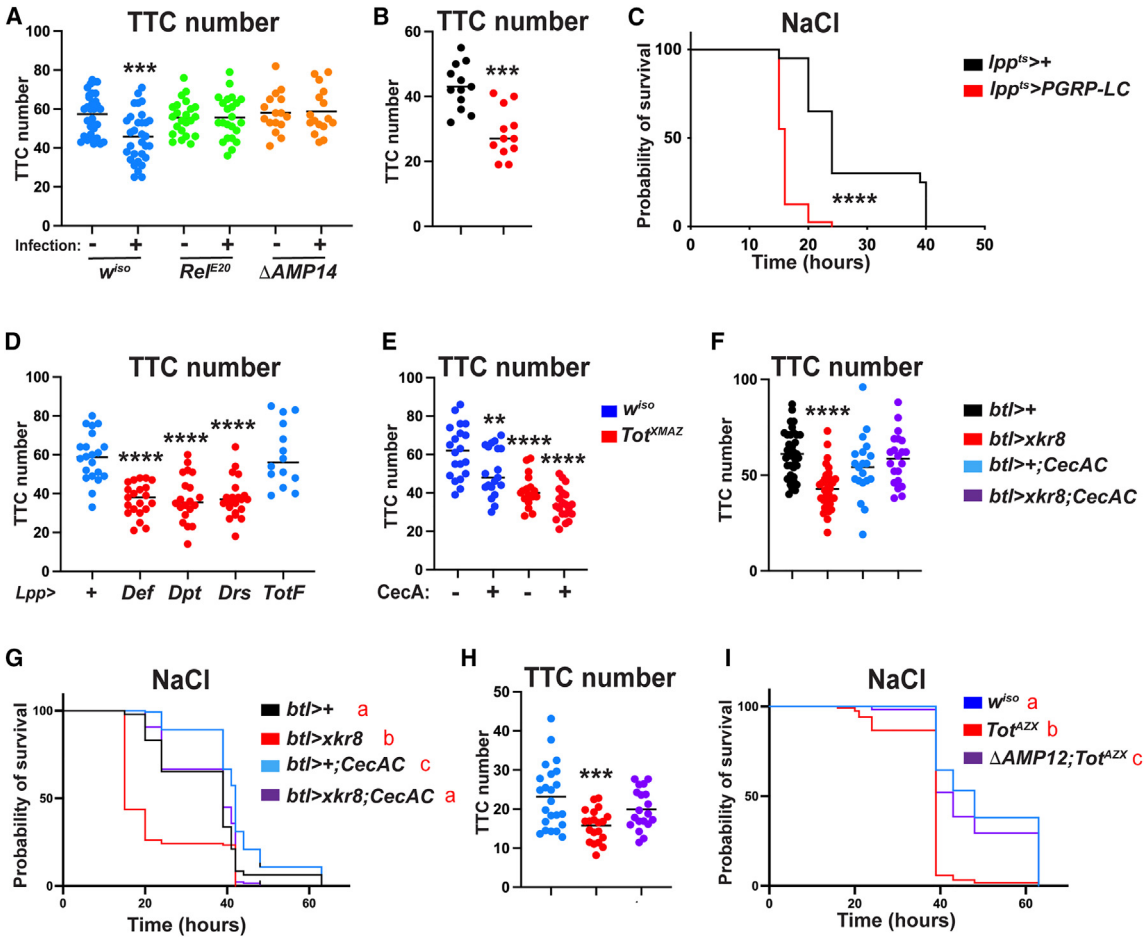


Figure 5. TotA prevents PS-dependent apoptosis of trachea by antimicrobial peptides

(A) Quantification of TTC numbers of w^{iso} (blue), Rel^{E20} (green), and *ΔAMP14* (orange) flies unchallenged or injured with a mixture of heat-killed *Micrococcus luteus* and *Ecc15*.

(B and C) Quantification of TTC numbers (B) and survival to osmotic stress (C) of flies overexpressing *PGRP-LC* in the fat body with the lpp^{ts} driver.

(D) Quantification of TTC numbers of flies with fat body overexpression of Defensin (*Def*), Diptericin (*Dpt*), Drosomycin (*Drs*), or *TotF* as a control.

(E) Quantification of TTC numbers of w^{iso} (blue) or Tot^{XMAZ} (red) flies injected with PBS or Cecropin A (CecA).

(F and G) A deletion removing four *Cecropin* genes (*CecAC*) rescues TTC numbers (F) and survival to osmotic stress (G) of flies overexpressing *xkr8*.

(H and I) Quantification of TTC number (H) and survival to osmotic stress (I) of w^{iso} (blue), Tot^{AZX} (red), and $ΔAMP12;Tot^{AZX}$ (purple) flies. Statistics: ordinary one-way ANOVA followed by a Dunnett's multiple comparisons test (A, D, F, and H); two-way ANOVA (E, $p = 0.001$ for treatment, $p < 0.0001$ for genotype), with no significant interaction between these factors ($F(1, 72) = 0.6015$, $p = 0.4406$). Mann-Whitney test (B); CoxPH test followed by Benjamini-Hochberg correction (C, G, and I). ** for p between 0.01 and 0.05; *** for p between 0.01; and 0.001, ****$p \leq 0.0001$.

flies. Strikingly, tracheation and resilience to osmotic stress in $ΔAMP12, Tot^{AZX}$ flies were similar to those observed in wild-type flies (Figures 5H and 5I). We conclude that Tot proteins mitigate damage caused by AMPs to tracheal cells exposing PS.

TotA prevents AMP-dependent pore formation

Previous studies have shown that AMPs can be cytotoxic to host cells in certain contexts.[4,37] We therefore explored whether Tot proteins could protect host cells from AMP activity *in vitro*, focusing on TotA. Electrophysiology recordings on artificial lipid bilayers mimicking eukaryotic membranes confirmed that the antibacterial peptide CecA made transient pores in PS-rich membranes,[38–40] while an unrelated control peptide (IM12 derived from the Baramicin A gene[41]) had no effect (Figures 6A and 6C). Strikingly, addition of TotA abrogated CecA-induced pore formation (Figures 6B and 6C). This result was confirmed in a liposome leakage assay. CecA but not IM12 induced liposome permeabilization. Addition of TotA was sufficient to completely abolish CecA-induced liposome leakage. This effect was specific to TotA as RNaseA, a protein of comparable molecular weight, did not impair CecA pore-forming activity (Figure 6D).

In addition to its antimicrobial activity, the human AMP LL37 has potent antitumoral properties, being capable of killing HL60 human leukemia cells.[42] We explored the impact of TotA on both LL37 microbicidal and antitumoral activities. TotA did not affect LL37 antibacterial activity on *Escherichia coli* (Figure 6E). However, HL60 cells treated with a mixture of LL37 and TotA had higher viability than cells treated with LL37 only,

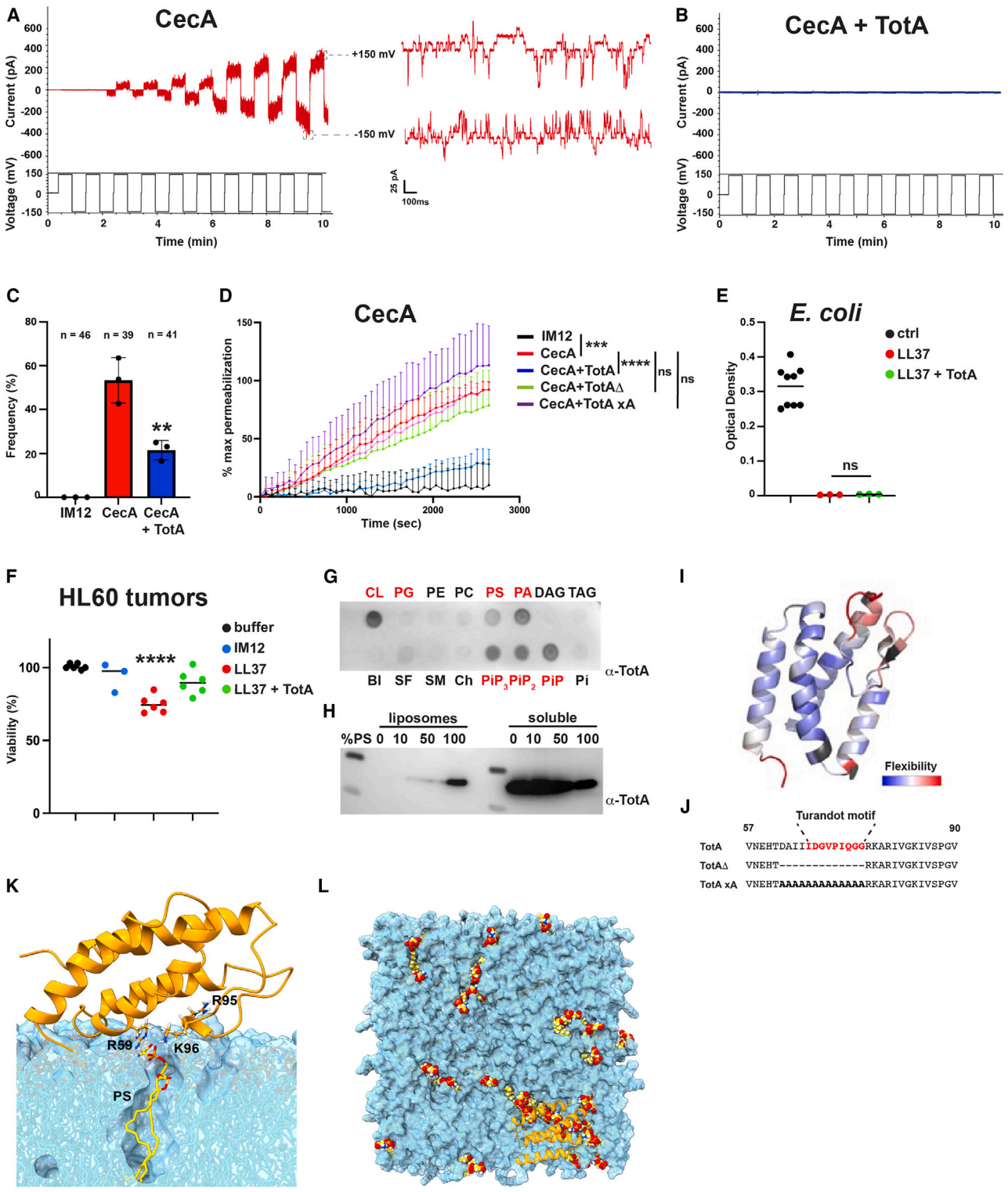


Figure 6. TotA prevents pore formation by AMPs

(A–C) Current recordings through lipid bilayer after addition of 8 μM CecA (A) or CecA + TotA (1:2) (B). Right panels in (A) show magnified current recordings at positive (upper) and negative (lower) voltages. (C) Quantification of pore frequency on artificial bilayers after addition of 8 μM IM12 (black), CecA (red), or CecA + TotA (1:2, blue). Shown are percentages of membranes with pores of 3 independent experiments (n values above the histogram represent total numbers of membranes measured).

(legend continued on next page)

showing that TotA inhibited LL37 activity specifically against eukaryotic cells (Figure 6F). These data indicate that TotA directly inhibits the activity of AMPs specifically on host cells.

TotA protects host cells from AMPs by sequestering PS

To address the biophysical mechanism underlying AMP inhibition by TotA, we next tested whether TotA could sequester CecA or LL37 in solution. Isothermal titration calorimetry did not reveal any interaction between these AMPs and TotA in solution (Figures S5A–S5D). Therefore, we explored whether TotA could interact with membrane bilayers. Electrophysiology recordings revealed a transient membrane disruption after TotA addition, suggesting a dynamic interaction of TotA with membranes (Figure S5E). We next tested whether TotA could bind to phospholipids using a lipid overlay assay. Strikingly, TotA binding was restricted to negatively charged phospholipids, with the exception of the bacterial lipid phosphatidylglycerol (PG) (Figure 6G). Accordingly, TotA protein bound to liposomes in a PS-dependent manner, further confirming that TotA interacts with negatively charged phospholipids (Figure 6H).

We then took a structural approach to explore how TotA interacted with membranes. The solution structure of TotA as determined by NMR revealed a four-helix bundle with an internal disordered loop between helix 3 and 4 (Figure 6I; PDB: 8PBV). This loop was less defined than the rest of the protein, likely because several residues at and around the loop were dynamic across a wide range of timescales (Figures 6I and S5F–S5H). This flexible loop contains the so-called Turandot motif (*[I/V]-D-G-v-p-x-Q-G-G*), which is shared by all Tot members[16] (Figure 6J). We hypothesized that this flexible loop may be important for TotA-mediated AMP inhibition. To test this hypothesis, we designed two protein variants where the loop was deleted (TotAΔ) or entirely replaced with alanines (TotAxA) (Figure 6J). Strikingly, both TotA variants were unable to prevent AMP-induced liposome lysis by CecA, in line with the idea that the loop is necessary for AMP inhibition (Figure 6D).

We then performed molecular dynamics (MD) simulations of TotA by placing it on the surface of a lipid bilayer model. TotA spontaneously reoriented itself on the membrane, with the Turandot motif loop facing the membrane surface (Figure 6K; Video S1). Strikingly, TotA displayed longer residence times around PS when compared with phosphatidylethanolamine (PE) or phosphatidylcholine (PC) lipids, despite PS representing only 10% of the membrane lipid composition (Figures S5J and S5K). Three positively charged TotA residues, R59 in helix 2 and R95 and K96 adjacent to the Turandot motif, individually contributed the most to PS binding during the simulations (Figure 6L), as assessed by their residence times and occupancy percentage (Figures S5J and S5K). This set of interactions triggered a clustering of PS around TotA (Figure 6L; Video S1). In contrast TotA did not co-localize as frequently with PC and PE (Figures S5L and S5M). Collectively, these results suggest that TotA can sequester PS, thereby preventing PS interaction with AMPs and subsequently preserving membrane integrity.

DISCUSSION

In this article, we provide evidence that Turandot proteins promote stress resilience in *Drosophila* by protecting host tissues from AMP-dependent lysis. Strikingly, we observed that TotA neutralizes the pore-forming activity of CecA and LL37 on host cells without impacting their microbicidal activity. TotA binds *in vivo* to tracheal cells and can interact with PS-enriched artificial membranes *in vitro*. MD simulations and lipid binding assays show that TotA preferentially interacts with PS, clustering and masking this phospholipid. We hypothesize that PS recruitment and sequestration by TotA shields PS from AMPs, thereby preventing AMP recruitment at the membrane. This would explain the broad protective effect of TotA against phylogenetically distant AMPs. By selectively inhibiting pore formation on eukaryotic cells, Turandot proteins increase AMP selectivity, allowing production of microbicidal AMPs at high concentrations while reducing collateral damage to host tissues. However, we cannot exclude that Tots protect from other molecules or processes targeting PS-enriched membranes in addition to AMPs. For instance, it would be interesting to test whether Turandot prevent PS-dependent phagocytosis.

Surprisingly, annexin V staining reveals that tracheal cells constitutively expose high levels of PS in the outer leaflet of the membrane. High PS exposure reduces the asymmetry between the inner and outer leaflet of the membrane and is thought to facilitate cell deformation and prevent shear stress.[43,44] This could be especially important in tracheal branches that are intimately attached to motile tissues, including the muscles and

(D) Kinetics of calcein leakage from liposomes incubated with 0.5 μM IM12 (black); CecA alone (red); or in combination with 1 μM TotA (blue), TotAΔ (green), or TotAxA (purple). Lines represent averaged values of 4 independent experiments with standard deviations.
(E and F) Viability of *E. coli* (E) and HL60 cells (F) after incubation with buffer (black), IM12 (blue, only in F), LL37 (red), or TotA + LL37 (green). Peptide concentrations used were 2 μM in (E) and 40 μM in (F). Shown are median (bar) and individual values of at least 3 independent experiments; error bars represent the SD.
(G) Representative membrane of a lipid overlay assay incubated with TotA and revealed by anti-TotA antibody. CL, cardiolipin; PG, phosphatidylglycerol; PE, phosphatidylethanolamine; PC, phosphatidylcholine; PS, phosphatidylserine; PA, phosphatidic acid; DAG, diacylglycerol; TAG, triacylglycerol; PI, phosphatidylinositol; PiP, phosphatidylinositol (4)-phosphate; PiP_2, phosphatidylinositol (4,5)-bisphosphate; PiP_3 phosphatidylinositol (3,4,5)-trisphosphate; Ch, cholesterol; SM, sphingomyelin; SF, 3-sulfogalactosylceramide; Bl, blank. Negatively charged lipids are highlighted in red.
(H) Anti-TotA western blot analysis of liposome-containing and soluble fractions after incubation of TotA with liposomes containing increasing amounts of PS.
(I) TotA structure as determined by NMR. Mapping of ^{1}H-^{15}N heteronuclear nuclear overhauser effect (NOE) onto the NMR structure of TotA, where red hints at more dynamic regions.
(J) Sequences of TotA from position 57 to 90 containing the Turandot motif (in red) and two variants with this motif deleted (TotAΔ) or alanine-replaced (TotAxA).
(K) Most representative binding conformation of TotA (orange cartoon) interacting with PS (yellow and red sticks) during the MD simulations. Most relevant charged residues for PS specificity are shown in sticks (blue, PE and PC).
(L) Representative snapshot of the MD simulation showing a lipid bilayer (blue) with some PS lipids (yellow and red spheres) clustering beneath TotA (orange cartoon). Statistics: (C) Fisher's exact t test, **p = 0.0057; (D) mixed-effects model with Geisser-greenhouse correction followed by uncorrected Fisher's LSD; (E) Mann-Whitney; (F) Kruskal-Wallis followed by a Dunn's test ***$p \leq 0.0005$; ****$p \leq 0.0001$.
See also Figure S5, Table S2, and Video S1.

gut, and are constantly exposed to mechanical stress.[28] We believe that Tots emerged through evolution to protect trachea and other tissues that are sensitized to lysis by AMPs due to reduced membrane asymmetry.

Restoration of homeostasis upon stress is energetically costly and requires increased respiration. That lethality of *Tot*-deficient flies with reduced tracheation can be rescued by hyperoxia illustrates that tissue oxygenation by trachea is critical to survive osmotic stress. We observed that susceptibility of Tot^{XMAZ} flies to infection is uncovered specifically in hypoxic conditions, indicating that oxygen delivery can also be a limiting factor in fueling the immune response. We speculate that the oxygen levels needed to mount a stress response depend on the nature of the stress: while osmotic stress requires high amounts of ATP (and therefore oxygen), immune responses may be less demanding in aerobic respiration. This would explain why *Tot*-deficient flies are overall resistant to bacterial infection in normoxic conditions.

We suspect that both basal and stress-induced Tot expression by epithelia and the fat body protect the respiratory epithelium. During pupariation, larval trachea undergo histolysis and adult trachea arise from pupal progenitors. Interestingly, both Tots and AMPs are highly expressed during this stage.[16,45] AMPs are expected to play a prophylactic role during this stage to prevent infection by bacteria escaping the gut during metamorphosis.[46] The fact that *Tot*-deficient adult flies emerge with a reduced tracheal cell number while larvae have normal tracheation is consistent with a protective role of Tots during pupariation. Future studies should explore the developmental roles of Tots.

Reports increasingly indicate that AMPs and other cationic peptides can be cytotoxic to host cells in certain contexts,[7–9] notably in neurodegeneration.[47] High PS exposure has also been associated with axon degeneration.[32] Here, we show that exposure of PS[48,49] upon stress or in certain cell types sensitizes them to cationic AMPs. It is therefore tempting to speculate that high PS exposure in neurons could sensitize this tissue to AMP-mediated killing. To our knowledge, our study is the first to identify a class of molecules protecting animal cells from the action of AMPs. Similar mechanisms might exist in other organisms, as suggested by an *in vitro* study showing that two well-known AMPs, LL37 and HNP1b, cooperate to kill bacteria more efficiently while minimizing mammalian cell membrane lysis.[50] Identification of factors such as Turandots that protect host cells from AMPs is therefore of therapeutic interest in several contexts, including neurodegeneration.

STAR★METHODS

Detailed methods are provided in the online version of this paper and include the following:

- KEY RESOURCES TABLE
- RESOURCE AVAILABILITY
  - Lead contact
  - Materials availability
  - Data and code availability
- EXPERIMENTAL MODEL AND SUBJECT DETAILS
  - Drosophila stocks and genetics
  - Survival experiments
  - Fly injections
- METHOD DETAILS
  - Cloning and DNA constructs
  - Recombinant protein and antibody production
  - Microbial cultures
  - Western blot
  - Immunostaining and trachea imaging
  - Trachea quantification
  - TUNEL staining
  - Tissue oxygenation determination
  - Image analysis and TTC quantification
  - Respirometry
  - NMR spectroscopy
  - Peptides
  - Isothermal titration calorimetry
  - Liposome preparation, binding, and leakage experiments
  - Lipid overlay assay
  - Single-channel bilayer experiments
  - Killing assays
- QUANTIFICATION AND STATISTICAL ANALYSIS
  - Structure assignment
  - Molecular dynamics simulation
  - Statistical analysis

SUPPLEMENTAL INFORMATION

Supplemental information can be found online at https://doi.org/10.1016/j.cub.2024.02.049.

ACKNOWLEDGMENTS

We thank the Bloomington Stock Center in the USA and the Vienna Drosophila Resource Center for fly stocks; Jordi Casanova, Stefano de Renzis, and Chun Han for providing fly strains; the BioImaging & Optics Platform (BIOP) in EPFL for confocal microscopy; the Protein Production & Structure Core Facility (PTPSP) for TotA production and NMR analysis; Hannah Westlake and Florent Masson for comments and editing on the manuscript; and Robin Hofmeister for helping with statistical analyses. This work was supported by Swiss National Science Foundation Sinergia grant CRSII5_186397 (to B.L.), the Swiss National Science Foundation (310030_215073 to B.L. and 205321_192371 to M.D.P.), and the Novartis Foundation (532114 to B.L. and 532589 to C.C.)

AUTHOR CONTRIBUTIONS

S.R., A.C., J.F.B.J., C.V., C.C., and B.L. conceived the study. S.K. provided mutant flies. S.R., A.C., J.F.B.J., L.A.A., J.-P.B., F.T.P.M., V.R., and C.V. conducted the experiments and analyzed the data. B.L., C.C., M.S.D., and M.D.P. acquired funding. S.R. and B.L. administrated the project. B.L., C.C., and M.D.P. supervised the study. S.R., A.C., and B.L. wrote the initial draft and J.F.B.J., L.A.A., C.C., M.S.D., and M.D.P. reviewed and edited the manuscript.

DECLARATION OF INTERESTS

The authors declare no competing interests.

Received: August 15, 2023
Revised: December 18, 2023
Accepted: February 21, 2024
Published: March 13, 2024

REFERENCES

1. Pakos-Zebrucka, K., Koryga, I., Mnich, K., Ljujic, M., Samali, A., and Gorman, A.M. (2016). The integrated stress response. EMBO Rep. *17*, 1374–1395.
2. Medzhitov, R., Schneider, D.S., and Soares, M.P. (2012). Disease Tolerance as a Defense Strategy. Science *335*, 936–941.
3. Dantzer, R., Cohen, S., Russo, S.J., and Dinan, T.G. (2018). Resilience and immunity. Brain Behav. Immun. *74*, 28–42.
4. Hanson, M.A., and Lemaitre, B. (2020). New insights on Drosophila antimicrobial peptide function in host defense and beyond. Curr. Opin. Immunol. *62*, 22–30.
5. Lazzaro, B.P., Zasloff, M., and Rolff, J. (2020). Antimicrobial peptides: Application informed by evolution. Science *368*, eaau5480.
6. Zasloff, M. (2002). Antimicrobial peptides of multicellular organisms. Nature *415*, 389–395.
7. Bacalum, M., and Radu, M. (2015). Cationic Antimicrobial Peptides Cytotoxicity on Mammalian Cells: An Analysis Using Therapeutic Index Integrative Concept. Int. J. Pept. Res. Ther. *21*, 47–55.
8. Parvy, J.-P., Yu, Y., Dostalova, A., Kondo, S., Kurjan, A., Bulet, P., Lemaître, B., Vidal, M., and Cordero, J.B. (2019). The antimicrobial peptide defensin cooperates with tumour necrosis factor to drive tumour cell death in Drosophila. eLife *8*, e45061.
9. Iwasaki, T., Ishibashi, J., Tanaka, H., Sato, M., Asaoka, A., Taylor, D., and Yamakawa, M. (2009). Selective cancer cell cytotoxicity of enantiomeric 9-mer peptides derived from beetle defensins depends on negatively charged phosphatidylserine on the cell surface. Peptides *30*, 660–668.
10. Vance, J.E., and Steenbergen, R. (2005). Metabolism and functions of phosphatidylserine. Prog. Lipid Res. *44*, 207–234.
11. Birge, R.B., Boeltz, S., Kumar, S., Carlson, J., Wanderley, J., Calianese, D., Barcinski, M., Brekken, R.A., Huang, X., Hutchins, J.T., et al. (2016). Phosphatidylserine is a global immunosuppressive signal in efferocytosis, infectious disease, and cancer. Cell Death Differ. *23*, 962–978.
12. Imler, J.-L., and Bulet, P. (2005). Antimicrobial Peptides in Drosophila: Structures,Activities and Gene Regulation. In Chemical Immunology and Allergy, D. Kabelitz, and J.-M. Schröder, eds. (KARGER), pp. 1–21.
13. Marra, A., Hanson, M.A., Kondo, S., Erkosar, B., and Lemaitre, B. (2021). Drosophila Antimicrobial Peptides and Lysozymes Regulate Gut Microbiota Composition and Abundance. mBio *12*, e0082421.
14. Overend, G., Cabrero, P., Guo, A.X., Sebastian, S., Cundall, M., Armstrong, H., Mertens, I., Schoofs, L., Dow, J.A.T., and Davies, S.-A. (2012). The receptor guanylate cyclase Gyc76C and a peptide ligand, NPLP1-VQQ, modulate the innate immune IMD pathway in response to salt stress. Peptides *34*, 209–218.
15. Zheng, W., Rus, F., Hernandez, A., Kang, P., Goldman, W., Silverman, N., and Tatar, M. (2018). Dehydration triggers ecdysone-mediated recognition-protein priming and elevated anti-bacterial immune responses in Drosophila Malpighian tubule renal cells. BMC Biol. *16*, 60.
16. Ekengren, S., Tryselius, Y., Dushay, M.S., and Liu, G. (2001). A humoral stress response in Drosophila. Curr. Biol. *5*, 714–718.
17. Ekengren, S., and Hultmark, D. (2001). A Family of Turandot-Related Genes in the Humoral Stress Response of Drosophila. Biochem. Biophys. Res. Commun. *284*, 998–1003.
18. Agaisse, H., Petersen, U.-M., Boutros, M., Mathey-Prevot, B., and Perrimon, N. (2003). Signaling Role of Hemocytes in Drosophila JAK/STAT-Dependent Response to Septic Injury. Dev. Cell *5*, 441–450.
19. Brun, S., Vidal, S., Spellman, P., Takahashi, K., Tricoire, H., and Lemaitre, B. (2006). The MAPKKK Mekk1 regulates the expression of Turandot stress genes in response to septic injury in Drosophila. Genes Cells *11*, 397–407.
20. West, C., and Silverman, N. (2018). p38b and JAK-STAT signaling protect against Invertebrate iridescent virus 6 infection in Drosophila. PLoS Pathog. *14*, e1007020.
21. Amstrup, A.B., Bæk, I., Loeschcke, V., and Givskov Sørensen, J. (2022). A functional study of the role of Turandot genes in Drosophila melanogaster: An emerging candidate mechanism for inducible heat tolerance. J. Insect Physiol. *143*, 104456.
22. Manenti, T., Loeschcke, V., and Sørensen, J.G. (2018). Constitutive up-regulation of Turandot genes rather than changes in acclimation ability is associated with the evolutionary adaptation to temperature fluctuations in Drosophila simulans. J. Insect Physiol. *104*, 40–47.
23. Linneweber, G.A., Jacobson, J., Busch, K.E., Hudry, B., Christov, C.P., Dormann, D., Yuan, M., Otani, T., Knust, E., de Bono, M., et al. (2014). Neuronal Control of Metabolism through Nutrient-Dependent Modulation of Tracheal Branching. Cell *156*, 69–83.
24. Nussbaumer, U., Halder, G., Groppe, J., Affolter, M., and Montagne, J. (2000). Expression of the blistered/DSRF gene is controlled by different morphogens during Drosophila trachea and wing development. Mech. Dev. *96*, 27–36.
25. Leader, D.P., Krause, S.A., Pandit, A., Davies, S.A., and Dow, J.A.T. (2018). FlyAtlas 2: a new version of the Drosophila melanogaster expression atlas with RNA-Seq, miRNA-Seq and sex-specific data. Nucleic Acids Res. *46*, D809–D815.
26. Perochon, J., Yu, Y., Aughey, G.N., Medina, A.B., Southall, T.D., and Cordero, J.B. (2021). Dynamic adult tracheal plasticity drives stem cell adaptation to changes in intestinal homeostasis in Drosophila. Nat. Cell Biol. *23*, 485–496.
27. Tamamouna, V., Rahman, M.M., Petersson, M., Charalambous, I., Kux, K., Mainor, H., Bolender, V., Isbilir, B., Edgar, B.A., and Pitsouli, C. (2021). Remodelling of oxygen-transporting tracheoles drives intestinal regeneration and tumorigenesis in Drosophila. Nat. Cell Biol. *23*, 497–510.
28. Hayashi, S., and Kondo, T. (2018). Development and Function of the *Drosophila* Tracheal System. Genetics *209*, 367–380.
29. Lidsky, P.V., Lukyanov, K.A., Misra, T., Handke, B., Mishin, A.S., and Lehner, C.F. (2018). Genetically-encoded fluorescent probe for imaging of oxygenation gradients in living *Drosophila*. Development *145*, dev156257.
30. Vucic, D., Kaiser, W.J., Harvey, A.J., and Miller, L.K. (1997). Inhibition of Reaper-induced apoptosis by interaction with inhibitor of apoptosis proteins (IAPs). Proc. Natl. Acad. Sci. USA *94*, 10183–10188.
31. Tanaka, K., Fujimura-Kamada, K., and Yamamoto, T. (2011). Functions of phospholipid flippases. J. Biochem. *149*, 131–143.
32. Sapar, M.L., Ji, H., Wang, B., Poe, A.R., Dubey, K., Ren, X., Ni, J.Q., and Han, C. (2018). Phosphatidylserine Externalization Results from and Causes Neurite Degeneration in Drosophila. Cell Rep. *24*, 2273–2286.
33. Tornesello, A.L., Borrelli, A., Buonaguro, L., Buonaguro, F.M., and Tornesello, M.L. (2020). Antimicrobial Peptides as Anticancer Agents: Functional Properties and Biological Activities. Molecules *25*, 2850.
34. Hedengren, M., Asling, B., Dushay, M.S., Ando, I., Ekengren, S., Wihlborg, M., and Hultmark, D. (1999). Relish, a Central Factor in the Control of Humoral but Not Cellular Immunity in Drosophila. Mol. Cell *4*, 827–837.
35. Carboni, A.L., Hanson, M.A., Lindsay, S.A., Wasserman, S.A., and Lemaitre, B. (2022). Cecropins contribute to *Drosophila* host defense against a subset of fungal and Gram-negative bacterial infection. Genetics *220*, iyab188.
36. Kylsten, P., Samakovlis, C., and Hultmark, D. (1990). The cecropin locus in Drosophila; a compact gene cluster involved in the response to infection. EMBO J. *9*, 217–224.
37. Gosztyla, M.L., Brothers, H.M., and Robinson, S.R. (2018). Alzheimer's Amyloid-β is an Antimicrobial Peptide: A Review of the Evidence. J. Alzheimers Dis. *62*, 1495–1506.
38. Cerón, J.M., Contreras-Moreno, J., Puertollano, E., de Cienfuegos, G.Á., Puertollano, M.A., and de Pablo, M.A. (2010). The antimicrobial peptide cecropin A induces caspase-independent cell death in human promyelocytic leukemia cells. Peptides *31*, 1494–1503.
39. Gazit, E., Boman, A., Boman, H.G., and Shai, Y. (1995). Interaction of the Mammalian Antibacterial Peptide Cecropin P1 with Phospholipid Vesicles. Biochemistry *34*, 11479–11488.

40. Suttmann, H., Retz, M., Paulsen, F., Harder, J., Zwergel, U., Kamradt, J., Wullich, B., Unteregger, G., Stöckle, M., and Lehmann, J. (2008). Antimicrobial peptides of the Cecropin-family show potent antitumor activity against bladder cancer cells. BMC Urol. *8*, 5.

41. Hanson, M.A., Cohen, L.B., Marra, A., Iatsenko, I., Wasserman, S.A., and Lemaitre, B. (2021). The Drosophila Baramicin polypeptide gene protects against fungal infection. PLOS Pathog. *17*, e1009846.

42. Fabisiak, A., Murawska, N., and Fichna, J. (2016). LL-37: Cathelicidin-related antimicrobial peptide with pleiotropic activity. Pharmacol. Rep. *68*, 802–808.

43. Shiomi, A., Nagao, K., Yokota, N., Tsuchiya, M., Kato, U., Juni, N., Hara, Y., Mori, M.X., Mori, Y., Ui-Tei, K., et al. (2021). Extreme deformability of insect cell membranes is governed by phospholipid scrambling. Cell Rep. *35*, 109219.

44. Nagao, K., and Umeda, M. (2023). Cellular function of (a)symmetric biological membranes. Emerging Top. Life Sci. *7*, 47–54.

45. Tryselius, Y., Samakovlis, C., Kimbrell, D.A., and Hultmark, D. (1992). CecC, a cecropin gene expressed during metamorphosis in Drosophila pupae. Eur. J. Biochem. *204*, 395–399.

46. Nunes, C., Koyama, T., and Sucena, É. (2021). Co-option of immune effectors by the hormonal signalling system triggering metamorphosis in Drosophila melanogaster. PLoS Genet. *17*, e1009916.

47. Smith, K.J., and Gwyer Findlay, E. (2022). Expression of antimicrobial host defence peptides in the central nervous system during health and disease. Discov. Immunol. *1*, kyac003.

48. Park, Y.-J., Kim, S., Shim, H.-P., Park, J.H., Lee, G., Kim, T.-Y., Jo, M.-C., Kwon, A.-Y., Lee, M., Lee, S., et al. (2021). Phosphatidylserine synthase plays an essential role in glia and affects development, as well as the maintenance of neuronal function. iScience *24*, 102899.

49. Kim, H.-Y., Huang, B.X., and Spector, A.A. (2014). Phosphatidylserine in the brain: Metabolism and function. Prog. Lipid Res. *56*, 1–18.

50. Drab, E., and Sugihara, K. (2020). Cooperative Function of LL-37 and HNP1 Protects Mammalian Cell Membranes from Lysis. Biophys. J. *119*, 2440–2450.

51. Basset, A., Khush, R.S., Braun, A., Gardan, L., Boccard, F., Hoffmann, J.A., and Lemaitre, B. (2000). The phytopathogenic bacteria Erwinia carotovora infects Drosophila and activates an immune response. Proc. Natl. Acad. Sci. USA *97*, 3376–3381.

52. Neyen, C., Bretscher, A.J., Binggeli, O., and Lemaitre, B. (2014). Methods to study Drosophila immunity. Methods *68*, 116–128.

53. Schindelin, J., Arganda-Carreras, I., Frise, E., Kaynig, V., Longair, M., Pietzsch, T., Preibisch, S., Rueden, C., Saalfeld, S., Schmid, B., et al. (2012). Fiji: an open-source platform for biological-image analysis. Nat. Methods *9*, 676–682.

STAR★METHODS

KEY RESOURCES TABLE

REAGENT or RESOURCE	SOURCE	IDENTIFIER
Antibodies		
chicken anti-GFP	Abcam	Cat# ab13970; RRID: AB_300798
Rat monoclonal anti-HA tag	Roche	Cat# 3F10; RRID: AB_2314622
Goat anti-Chicken IgY (H+L) Secondary Antibody, Alexa Fluor 488	Thermo Fischer Scientific	Cat# A11039; RRID: AB_2534096
Goat anti-Rat IgG (H+L) Cross-Adsorbed Secondary Antibody, Alexa Fluor 555	Thermo Fischer Scientific	Cat# A21434; RRID: AB_2535855
Goat anti-Rabbit IgG (H+L) Highly Cross-Adsorbed Secondary Antibody, Alexa Fluor 555	Thermo Fischer Scientific	Cat# A21428; RRID: AB_2535849
Rabbit polyclonal anti-TotA antibody	This study	N/A
Rabbit monoclonal anti-Cleaved Caspase-3	Cell Signaling	Cat# 9664; RRID: AB_2070042
Peroxidase-AffiniPure Donkey Anti-Rabbit IgG (H+L)	Jackson ImmunoResearch Labs	Cat# 711-035-152; RRID: AB_10015282
Goat anti-Mouse IgG (H+L) Highly Cross-Adsorbed Secondary Antibody, Alexa Fluor 555	Thermo Fischer Scientific	Cat# A21424; RRID: AB_141780
Bacterial and virus strains		
Erwinia carotovora carotovora15	Basset et al.[51]	N/A
Micrococcus luteus	Neyen et al.[52]	N/A
Enterococcus faecalis	ATCC 29212	29212
Drosophila C Virus	Pr. Carla Saleh (Pasteur Institute)	N/A
Chemicals, peptides, and recombinant proteins		
Recombinant TotA WT	This study	N/A
Recombinant TotA xA	This study	N/A
Recombinant TotA delta	This study	N/A
4',6-Diamidino-2-phenylindole dihydrochloride (DAPI)	Sigma	Cat# D9542; CAS: 28718-90-3
complete protease inhibitor	Sigma	11697498001
phenylmethylsulfonyl fluoride	Sigma	P7626
Paraformaldehyde 16% solution, EM grade	Electron Microscopy Sciences	Cat# 15710
CecropinA	Sigma	C6830
Melittin	Sigma	C6830
CecropinA	GenicBio	N/A
LL37	GenicBio	N/A
Calcein	Sigma	C0875
DOPS	Sigma	840035
DOPE	Sigma	850725
DOPC	Sigma	850375
Critical commercial assays		
In Situ Cell Death Detection Kit, TMR red	Roche	12156792910
Membrane lipid strips	Echelon Bioscience	P-6002
Deposited data		
TotA NMR Structure		PDB: 8PBV
Experimental models: Cell lines		
Human leukemia-60 (HL-60)	ATCC	CCL-240
S2 cells	ATCC	CRL-1963
Experimental models: Organisms/strains		
See Table S1. Stocks used in this study	N/A	N/A

(*Continued on next page*)

CellPress
OPEN ACCESS

Continued

REAGENT or RESOURCE	SOURCE	IDENTIFIER
Recombinant DNA		
pET32b-TotA	This study	N/A
pET32b-TotAxA	This study	N/A
pET32b-TotAdelta	This study	N/A
Software and algorithms		
Fiji	Schindelin et al.[53]	http://www.fiji.sc/
Prism 5	GraphPad	https://www.graphpad.com/scientificsoftware/prism/
Geneious	Geneious	N/A

RESOURCE AVAILABILITY

Lead contact

Further information and requests for resources and reagents should be directed to and will be fulfilled by the lead contact, Bruno Lemaitre (bruno.lemaitre@epfl.ch)

Materials availability

Drosophila stocks and antibodies generated in this study will be available upon request to the authors.

Data and code availability

TotA structure has been deposited and is available as of the date of publication in PDB: 8PBV and NMR chemical shifts at the BMRB: 34825. All data reported in this paper will be shared by the lead contact upon request. This paper does not report original code. Any additional information required to reanalyze the data reported in this paper is available from the lead contact upon request.

EXPERIMENTAL MODEL AND SUBJECT DETAILS

Drosophila stocks and genetics

Flies were raised on Yeast-Cornmeal food (6% cornmeal, 6% yeast, 0.62% agar, 0.1% fruit juice, supplemented with 10.6g/L Moldex and 4.9ml/L propionic acid) at 25°C. Experiments were performed on 5-10 days old animals at 25°C, unless otherwise stated. Animals were bred and maintained at a low population density in vials and flipped twice a week. Isogenic w^{1118} Drosdel flies [S2] (w^{iso}) were used as wild type. *TotM* and *TotX* mutants were generated as previously described [S10]. Briefly, w^{iso} embryos were injected with a mixture of recombinant Cas9 (Invitrogen) and a gRNA targeting the *TotM* coding sequence (ACTTATCGTAGAAAGTGACCAGG) or the *TotX* coding sequence (GTTCAAGTTATGAGGAACACAGG), respectively. $TotAZ^{sk6}$ line was created as previously described in [S11]. This mutation was subsequently backcrossed in the w^{iso} background. To generate Tot^{AZX} stock, $TotAZ^{sk6}$ embryos were injected with a mixture of recombinant Cas9 (Invitrogen) and a gRNA targeting TotX coding sequence (GTTCAAGTTATGAGGAACACAGG). Tot^{AZX} mutations were then combined with *TotM* mutation (on the second chromosome) to create the Tot^{XMAZ} line. All Tot^{AZX} mutations were located on the third chromosome and this mutant almost phenocopied Tot^{XMAZ}. Additionally, most of the transgenes and genomic deletions used in our genetic analysis were located on the second chromosome. We therefore decided to use Tot^{AZX} instead of Tot^{XMAZ} in this study in order to simplify the genetic schemes. *UAS-TotA-HA* and *UAS-HA-TotA* lines were generated by phiC3-mediated recombineering. Stocks used in this study are listed in Table S1.

Survival experiments

All experiments were done on 5- to 7-days old adult flies. Systemic infections with *Ecc15*, *Micrococcus luteus* and *Enterococcus faecalis* were performed as follows [S12]: female flies were pricked in the thorax with a needle previously dipped into a concentrated bacterial pellet at OD_{600}:200 (*Ecc15* and *M. luteus*) or OD_{600}:5 (*E. faecalis*). Infected flies were maintained at 25°C (*E. faecalis*) or 29°C (*Ecc15* and *M. luteus*) and survival was recorded daily. Flies were flipped into fresh vials every 2-3 days. Infections in a hypoxic environment (8% O_2) were performed at 29°C on male flies. Systemic infections with DCV were performed by injecting 50 nL of $2*10^5$ $TCID_{50}$/mL into the thorax of female adult flies using a nanoinjector (Drummond) and glass capillary needles.

Survivals to abiotic stresses were performed as follows: osmotic stress experiments were performed by feeding on fly food supplemented with NaCl (final concentration: 4%). Male flies carrying Gal4 or $Gal4^{ts}$ driven transgenes were raised at 25°C, kept for 3 days at 25°C, transferred for 2-4 days to 29°C and exposed to an osmotic stress at 29°C (with the exception of experiments shown in Figure 1, where females flies were maintained at 25°C). Flies overexpressing *PGRP-LC* were raised at 18°C instead of 25°C. Starvation experiments were performed by keeping female flies on 1.8% agar. Rescue experiments of starvation were done on males. For

heat stress experiments, flies were kept in a 34°C incubator. For osmotic stress experiments in a hypoxic/hyperoxic environment, flies were maintained in an incubator with controlled oxygen levels (5% O_2 for hypoxia of 60% O_2 for hyperoxia).

Fly injections

Female flies were injected in the abdomen with 50nL of 100 μM synthetic CecA or heat-killed bacteria and guts were dissected 48h and 96h later, respectively. Injections with recombinant TotA were as follows: female flies were injected in the thorax with 23nL of 10μM or 450μM recombinant TotA for imaging and survival experiments, respectively.

METHOD DETAILS

Cloning and DNA constructs

Cloning was performed by Gibson assembly (New England Biolabs), following the manufacturer's instructions. *TotA* coding sequence was cloned into the pUASt-attb-GFP vector and a HA tag was added in C-term. A sequence containing the TotA 5'UTR, TotA signal peptide, 3 times HA-tag and TotA CDS was ordered from Genewiz and subsequently cloned into the pUASt-attb-GFP vector to create the UAS-HA-TotA construct. For recombinant protein expression, a codon-optimized version of TotA fused to a Tobacco Etch Virus (TEV) protease cleavage site was ordered from Twist Bioscience and cloned into the pET29b vector. TotAxA and TotAΔ were made by GenScript, using pET29b-TotA as a template.

Recombinant protein and antibody production

TotA, TotAxA and TotAΔ were expressed overnight at 18°C in Rosetta2 *E. coli* (DE3, Novagen). Cells were lysed by sonication in 700 mM NaCl; 20 mM HEPES 7.5 containing 1 protease inhibitor tablet (Roche) + 5 μl Turbonuclease. TotA was purified using HisPur Ni-NTA Resin beads (ThermoFisher). MBP protein was cut using super TEV protease and both proteins were removed using HisPur Ni-NTA Resin beads. TotA was further purified by incubation with Amylose Resin (New England Biolabs) followed by size-exclusion chromatography on a HiLoad superdex75 16/60 column (GE healthcare) and concentrated in 150 mM NaCl; 20 mM HEPES pH = 7.5. TotA was used as immunogen to produce rabbit anti-TotA antibody (made by GenScript).

Microbial cultures

Bacteria were cultured overnight on a shaking plate at 180 RPM. The following morning, they were pelleted by centrifugation (4000 RPM at 4°C) and the bacterial pellets were diluted to the desired optical density at 600nm (OD_{600}). *Pectobacterium carotovorum carotovorum 15* (*Ecc15*) and *Micrococcus luteus* were grown in LB medium at 29°C. *Enterococcus faecalis* was grown in GHI medium at 37°C. For experiments with heat killed bacteria, a mixture of *Ecc15* and *M. luteus* pellets (OD100 each) was cyclically (4 times) heated at 95°C and frozen at -20°C. *Drosophila C Virus* (*DCV*) stock was kindly provided by Prof. Carla Saleh.

Western blot

Total hemolymph was harvested by bleeding ten L3 wandering larvae in 100 μL of Phosphate Buffered Saline (PBS) supplemented with Complete Inhibitor (Roche, diluted 1/50), PMSF (1 mM) and PTU (1 mM). A step of centrifugation (5 min at 500 x g) was done to discard hemocytes. 10 μg of protein was denatured (2 min at 80°C) and then separated on a Novex 10-20% precast Tricine Gel and transferred to a nitrocellulose membrane (Invitrogen iBlot). The membrane was blocked in 5% non-fat dry milk in PBS containing 0.1% Tween-20 for 1 h and then incubated overnight at 4°C with a rabbit anti-TotA (1:1000 dilution) antibody. Goat anti-rabbit-HRP secondary antibody (Jackson ImmunoResearch) diluted at 1:15000 was incubated for 1 h at room temperature. Bound antibodies were detected using SURESIGNAL Western Substrate (LubioScience). The membrane was imaged on a ChemiDoc XRS+ (BioRad).

Immunostaining and trachea imaging

Guts were dissected in PBS and fixed in 8% paraformaldehyde for 15 min at room temperature. The tissues were subsequently rinsed two times with PBS containing 0.1% Triton X-100, blocked for 1 h in PBS containing 1% of goat serum and 2% BSA, and incubated at 4°C in the blocking solution containing an anti-GFP (2 h, 1:3000), anti-HA (overnight, 1:500) or anti-cleaved Caspase3 primary antibody (overnight, 1:500). The tissues were subsequently washed and incubated with a secondary antibody (1:4000) for 1 h at room temperature. After extensive washes, tissues were mounted in glycerol. Anti-TotA staining was done following a similar protocol without adding Triton X-100. To image AnnevinV-GFP, guts were dissected in AnnexinV buffer (Hepes 10mM, NaCl 150 mM, KCl 5 mM, $MgCl_2$ 5 mM, $CaCl_2$ 1.8 mM) and subsequently stained following the abovementioned protocol. Anti-TotA staining of fat bodies was performed on dissected carcasses. Tissues were fixed for 45 min, permeabilized in PBS-0.1% Triton X-100 for 1 h, blocked for 1 h in PBS containing 1% of goat serum and 2% BSA, and incubated overnight at 4°C in the blocking solution containing anti-TotA antibody (1:3000). The tissues were subsequently washed and incubated with a secondary antibody (1:4000) for 1 h at room temperature. After extensive washes, tissues were mounted in glycerol.

Trachea quantification

Tracheation of guts was assessed by imaging the autofluorescent chitin lining the tracheal lumen. The dityrosine bonds chitin fluoresce under UV excitation, allowing chitin to be imaged using a DAPI filter set. Female flies were raised as described for survival

experiments. 5-7 day old flies were maintained on control food or exposed to an osmotic stress for 20 h or 24 h and then starved for 2 h before guts were dissected and fixed in 8% paraformaldehyde for 45 min at room temperature. Guts were subsequently washed 3 times for 15 min in PBS and mounted in glycerol. Guts were imaged on a LSM700 microscope (Zeiss) using the DAPI channel.

TUNEL staining

Guts from adult female flies were dissected in PBS and fixed in 4% paraformaldehyde for 15 min at room temperature. The guts were subsequently rinsed three times with PBS and permeabilized for 2 min in PBS+0.1% Triton X-100 + 0.1% Sodium citrate tribasic dihydrate and rinsed three times in PBS. Guts were then incubated for 1 h with reagents from the *In Situ Cell Death Detection Kit, TMR red* (Roche). Tissues were washed three times and mounted in Dako Fluorescence Mounting Medium (Agilent).

Tissue oxygenation determination

Oxygenation of Drosophila tissues was determined using a genetically-encoded fluorescent probe (nls-timer) as described [S5]. Guts and Malpighian tubules were dissected and fixed in 4% paraformaldehyde for 45 min and mounted in glycerol. Images were acquired in the GFP and RFP channels on a Leica M205 FA fluorescent stereomicroscope. Ratiometric analysis of red and green nuclei fluorescence was performed using ImageJ to determine tissue oxygenation.

Image analysis and TTC quantification

Image quantifications were performed using ImageJ software. Trachea coverage was determined by measuring the surface of trachea divided by the area of the R2 gut region. Terminal tracheal cells cellular bodies, as defined by the characteristic shape of the chitinous lumen, were manually counted in the R2 region of the midgut.

Respirometry

Respiration in flies was measured using a stop-flow gas-exchange system (Q-Box RP1LP Low Range Respiration, Qubit Systems, Ontario, Canada, K7M 3L5). Eight female flies were put into an airtight glass tube and supplied with food. Each tube was provided with CO_2-free air while 'spent' air was simultaneously flushed through the system and analyzed for its CO_2 and O_2 content. In this way, evolved CO_2 and consumed O_2 were measured for each tube every $\sim$ 44 min for a duration of 12–16 h.

NMR spectroscopy

Recombinant proteins for NMR spectroscopy were prepared with the isotope enrichment scheme appropriate for each experiment in MES buffer pH 6 with 100 mM NaCl and 10% ^2H_2O. Protein concentrations were around 300 μM for NMR titrations and close to 1 mM for experiments aimed at resonance assignment, structure determination, and ^{15}N relaxation analysis. All NMR experiments were carried out in an 18.8 T (800 MHz ^1H Larmor frequency) Bruker spectrometer equipped with a CPTC ^1H,^{13}C,^{15}N 5 mm cryoprobe and an Avance Neo console. Backbone (H, N, CA, and C) and CB resonances were assigned using a standard procedure based in conventional 3D HNCA, HN(CO)CA, HNCO, HN(CA)CO, CBCA(CO)NH and HNCACB spectra, further assisted by ^{15}N-resolved TOCSY and NOESY [S13]. Experiments for sidechain assignment and structure calculation entailed ^{15}N-resolved NOESY, ^{15}N-resolved TOCSY, HCCH-TOCSY, ^{13}C-resolved NOESY, HNHA, 2D TOCSY and 2D NOESY spectra. All spectra were acquired and processed using Bruker's Topsin 4.0 software.

Peptides

Purified CecA (Sigma) was used in leakage experiments. Synthetic CecA, IM12 (pQFHVERPGRTVDVGNGGFYIQRG) and LL37 were purchased from GenicBio (purity> 95%).

Isothermal titration calorimetry

ITC experiments were performed on a Microcal PEAQ-ITC (Malvern Instruments). 2 μL of a 10 mM HEPES pH7.5 150 mM NaCl solution of 2μM CecA or LL37 was injected 13 times in the chamber containing 200 μM TotA and heats of reaction were recorded. Control experiments were run where peptides were titrated in the buffer solution alone.

Liposome preparation, binding, and leakage experiments

Lipids (3 mg) were resuspended in chloroform and mixed at a 3:1:0.4 ratio (DOPE:DOPC:DOPS). Chloroform was evaporated under a nitrogen stream and the lipid film was hydrated with 600 μL of 50 mM Tris pH=8, 100 mM NaCl containing 70 mM calcein. After 5 freeze-thaw cycles, liposomes were extruded 20 times through a 0.2 μm pore-size filter. To remove un-entrapped calcein, liposomes were passed through two HiTrap columns at low flow rate. Fractions containing calcein-loaded liposomes were pooled, diluted 4 times and used for subsequent assays. For calcein leakage experiments, 10 μl liposomes were incubated in 90 μl 50 mM Tris pH=8, 100 mM NaCl containing 0.5 μM TotA, TotAxA or TotAΔ, together with CecropinA (Sigma-Aldrich, at a concentration of 1 μM) and fluorescence was recorded on an Infinite M Nano fluorospectrophotometer (Tecan) for 1 h. Maximum release of Calcein was determined by addition of 0.1% Triton-X100 and data were normalized as percentage of full release. For binding assays, 3 μM TotA was incubated with 180 mL 1 mg/mL liposomes containing DOPC and increasing amounts of DOPS for 30 min at room temperature and centrifuged at 100000 x g in a discontinuous sucrose gradient (35%:20%:10%) for 1 h. Liposome fraction and soluble fractions were subjected to anti-TotA immunoblotting.

Lipid overlay assay

Membrane lipid strips (Echelon Bioscience) were incubated with 0.5 mg/mL TotA in PBS-0.1% Tween, 3%BSA for 1 h at room temperature. TotA was then probed with an anti-TotA antibody as described above.

Single-channel bilayer experiments

1,2-diphytanoyl-*sn*-glycero-3-phosphocholine (DPhPC) and 1,2-diphytanoyl-*sn*-glycero-3-phospho-L-serine powder (DPhPS) (Avanti Polar Lipids Inc.,) were dissolved in octane (Sigma-Aldrich) to a final concentration of 8 mg/mL and either used pure or in mixture as specified in the figure caption. Single-channel recording experiments were performed on an Orbit 16 TC instrument (Nanion). Phospholipid membranes were formed across a MECA 16 recording chip that contains 16 circular microcavities (100 μm diameter) in a highly inert polymer. Each cavity contains an individual integrated Ag/AgCl microelectrode and can record 16 artificial lipid bilayers in parallel. The buffer (10 mM HEPES, 200 mM KCl, pH=7.4), the concentration of CecA and TotA was 8 μM and the temperature was set to 25°C for all experiments. Membranes were formed and their capacitance were recorded (Figure S5). The traces were recorded in Elements Data Reader (Elements) and further analyzed by Clampfit (Molecular device). Data was collected at 20 kHz sampling rate with a 10 kHz low-pass filter. Results, fitting, and graphs were produced in Prism (GraphPad) and figures were generated in Adobe Illustrator 2022 (Adobe).

Killing assays

A culture of *E. coli* grown overnight was diluted to OD_{600}: 0.001 and allowed to regrow for 2 h at 29°C. 1 μl of this culture was diluted in 100 μL LB containing 2 μM LL37 in the absence or presence of 2.5 μM TotA. The plate was incubated at 25°C under intermittent agitation and OD was recorded every 10 min for 16 h. For eukaryotic cell killing assay, 10000 HL60 cells were seeded in 100 μL of RPMI supplemented with heat-inactivated FBS, HEPES and antibiotics in half-area 96-well plates (corning). The next day, 50 μL of supernatant was removed and LL37 and TotA were added at 40 and 80 μM final concentration, respectively. After 1 h of incubation at 37°C, 5 μL of MTT (Biotium) was dispensed in each well and further incubated at 37°C for 1 h. 100 μL DMSO was then added and thoroughly mixed to dissolve crystals. Absorbance was read at 570 nm and 630 nm on an Infinite M nano spectrofluorometer (Tecan).

QUANTIFICATION AND STATISTICAL ANALYSIS

Structure assignment

Backbone and sidechain assignments were obtained through manual spectral analysis assisted by the program CARA [S14]. Analysis of NOESY spectra and structure calculations were performed semiautomatically using UNIO's ATNOS/CANDID module coupled to Cyana [S15,S16] using NOEs and dihedral angles derived from chemical shifts with Talos-n [S17]. NMR structure statistics are provided in Table S2. The solved protein structure was deposited in the PDB: 8PBV and NMR chemical shifts at the BMRB: 34825.

For studies of ^{15}N relaxation, heteronuclear ^{1}H-^{15}N NOEs were measured using an interleaved, phase-sensitive gradient-enhanced version; and ^{15}N T_1 and T_2 were measured via conventional pseudo-3D experiments that apply respectively inversion recovery or CPMG sequences onto an HSQC spectrum, both using gradient selection, water suppression, and decoupling during acquisition. All spectra for measurement of ^{15}N relaxation were acquired with 256 increments in the indirect dimension and 3 s of relaxation delay. For T_1 measurements we used delays of 20, 50, 100, 200, 300, 400, 500, 700, 1000, 1200, 1500, 2000, 3000 and 4000 ms. For T_2 measurements we used delays of 17, 34, 51, 68, 85, 102, 119, 136, 170, 204, 238, 272 and 340 ms. Relaxation rates were fitted from exponential decay models using the ad hoc module from the Sparky-NMRfam program [S18] on the peaks derived from our backbone assignment.

Molecular dynamics simulation

We obtained the structure of TotA from the AlphaFold Protein Structure Database (AFDB) [S19,S20] under the UniProt accession code Q8IN44 [S21]. The models available in AFDB are computed based on the entire sequence of the target proteins, so it was necessary to remove the sequence peptide of TotA (residues 1 to 21) from the structure prior to preparing the simulation setup.

We processed the TotA model in the CHARMM-GUI web server [S22] to generate the input files for the MD simulation, using the CHARMM-GUI Membrane Builder tool [S23]. We used the Positioning of Proteins in Membrane (PPM) tool from Orientations of Proteins and Membranes (OPM) database to orient TotA with respect to the membrane [S24]. We generated a tetragonal box with TotA and a symmetric lipid bilayer with 10% DOPS, 30% DOPC, and 60% DOPE, resulting in a membrane with an area of 131 × 131 $Å^2$. We solvated the system with TIP3P water [S25] and neutralized its liquid charges with counterions corresponding to a 0.15 M NaCl solution. Lastly, we generated all the necessary files to run the MD simulations with the CHARMM36m forcefield [S26].

We used GROMACS [S27] version 2022.1 to run and analyze the MD simulations. In all stages of the procedure, the cutoff radius for short-range electrostatic and van der Waals interactions was 12 Å; we used the particle mesh Ewald algorithm (PME) [S28] to calculate long-range electrostatic interactions. We restrained the length of covalent bonds involving hydrogen atoms using the LINCS algorithm [S29]. Periodic boundary conditions were applied in all directions.

In the first stage of the simulation protocol, we minimized the potential energy of the system using the steepest descent algorithm, employing a 1000 kJ mol-1 nm-1 maximum force constant on the atoms as a convergence criterion. After minimization, we subjected the system to thermal equilibration in the canonical ensemble (NVT) [S30], to accommodate water and counterions around the protein

and membrane. Initial atomic velocities were determined following a Maxwell-Boltzmann distribution corresponding to a temperature of 300 K and we equilibrated the system under these conditions for 0.25 ns with a 1 fs time step using the Berendsen thermostat [S31]. During the equilibration stage, we restrained heavy-atom positions using a harmonic potential, with force constants of 4000 (backbone) and 2000 (sidechain) kJ mol-1 nm-2, respectively. The phosphorus atoms of the lipid molecules were also restrained on the Z-axis (direction of the normal vector at the membrane surface), as well as the dihedral angles of the double bonds in the fatty acid chains, with force constants of 1000 kJ mol-1 nm -2 and 1000 kJ mol-1 rad-2, respectively.

After controlling the temperature, we stabilized pressure and density in the isothermal-isobaric ensemble (NPT) [S32]. The pressure was maintained at 1 bar using the Berendsen barostat[31] with semi-isotropic pressure coupling and a 5 ps time constant. The systems were equilibrated for 1.625 ns, with position restraints released gradually.

The production dynamics were also performed in the NPT ensemble, changing only the thermostat used for Nosé-Hoover [S33,S34] and the barostat to Parrinello-Rahman [S35,S36]. This stage lasted 1 μs, with a time step of 2 fs. All simulations had five replicas and only the last 500 ns of each simulation were used for the analyses.

We performed all lipid interaction analyses with the Python package PyLipID [S37]. The distance cutoff for lipid interactions was set to 0.3 nm, and only residence times calculated with an estimated $R2 > 0.97$ were reported.

We used the Visual Molecular Dynamics (VMD) [S38] software for visual inspection of the simulations and recording of the Videos. All protein and membrane images were generated with ChimeraX [S39]. Density and violin plots were generated with the R programming language in RStudio [S40].

Statistical analysis

Each experiment was repeated independently at least three times. Survival curves included experiments with at least one cohort of 20 flies per condition. Survival analyses were performed using a Cox proportional hazards (CoxPH) model, with Benjamini-Hochberg correction for p values when multiple comparisons were done. In this case, statistics were represented using a compact letter display (CLD) graphical method: groups were assigned the same letter if they were not significantly different ($p > 0.05$). Quantification data were analyzed using a Mann-Whitney test, Welch two sample t test, student t test, ordinary one-way ANOVA with Dunnett's multiple comparisons test or two-way ANOVA, as stated in the figure legends. Error bars represent the standard deviation of the median of replicate experiments (SD). p values are represented in the figures by the following symbols: ns for $p \geq 0.05$, * for p between 0.01 and 0.05; ** for p between 0.001 and 0.01, *** for p between 0.0001 and 0.001, **** for $p \leq 0.0001$. Survival statistics were represented using a compact letter display graphical technique: groups were assigned the same letter if they were not significantly different ($p > 0.05$). All statistics are summarized in Table S3.